# Chiral Metafoils for Terahertz Broadband High-Contrast Flexible Circular Polarizers

Jianfeng Wu,[1,2] Binghao Ng,[3] Haidong Liang,[2,4] Mark B. H. Breese,[2,4] Minghui Hong,[1] Stefan A. Maier,[3] Herbert O. Moser,[5] and Ortwin Hess[3,*]

[1]*Department of Electrical and Computer Engineering, National University of Singapore, 4 Engineering Drive 3, 117576 Singapore, Singapore*

[2]*Department of Physics, Center for Ion Beam Applications (CIBA), National University of Singapore, 2 Science Drive 3, 117542 Singapore, Singapore*

[3]*The Blackett Laboratory, Department of Physics, Imperial College London, London SW7 2AZ, United Kingdom*

[4]*Singapore Synchrotron Light Source (SSLS), National University of Singapore, 4 Engineering Drive 3, 117576 Singapore, Singapore*

[5]*Karlsruhe Institute of Technology (KIT), Institute of Microstructure Technology (IMT), Postfach 3640, D-76021 Karlsruhe, Germany*

(Received 8 May 2014; published 18 July 2014)

Metamaterial concepts have opened the door to high-optical anisotropy beyond levels of naturally occurring materials but usually with limited spectral bandwidth. Here, we report on the design, realization, and experimental and numerical characterization of broadband chiral metafoils exhibiting at the same time exceptionally high-contrast circular polarization in the THz range. We demonstrate that the observed chirality is achieved by a simple modification of the structure of well-established metafoils, namely, through a shift of interconnecting lines by half a unit cell length between each row. The bandwidth of the observed circular-polarization-selective response is demonstrated to be up to about one octave at a center frequency of 2.4 THz and the ratio of the transmission of oppositely circularly polarized radiation is shown to reach about 700%, with the maximum transmittance being approximately 70%. Although implemented here at THz frequencies, broadband chiral metafoils may be extended to higher infrared and optical frequencies by hot embossing or nanoimprinting. They may be used as circular polarizers and beam stops in THz optical and infrared systems.

DOI: 10.1103/PhysRevApplied.2.014005

## I. INTRODUCTION

Circular optical dichroism, the differential absorption of right- and left-handed circularly polarized light, is a characteristic attribute of light and an important means of using light to study the structure and properties of chiral molecules [1]. While generally, 2D or 3D objects are called chiral if their mirror image at a line or a plane, respectively, cannot be transformed into the original by translations and/or rotations, many biologically relevant molecules such as naturally existing amino acids, enzymes, and sugars are chiral and chiral molecules are also of great importance in chemistry, biology, and pharmaceuticals. However, in naturally chiral molecules the chirality is relatively low. Not surprisingly, artificial chiral "molecules," such as helical coils, are thus studied with an aim to achieving augmented chiral effects [2,3]. Combining chirality with metamaterials, chiral metamaterials have recently attracted considerable attention due to their exotic properties, such as giant optical activity as well as their potential to realize materials with negative refraction [4–17]. In chiral metamaterials, strong magnetoelectric coupling gives rise to an appreciably different optical response of left-handed circularly polarized (LCP) and right-handed circularly polarized (RCP) light. On the basis of this concept, chiral metamaterials have opened a new route to building circular polarizers with octave-wide frequency ranges of operation.

For conventional circular polarizers, two methods have commonly been used to generate circularly polarized light: (1) Bragg reflection using a cholesteric liquid-crystal film and (2) a linear polarizer laminated with a quarter-wave film [18]. However, their narrow-band response at an *a priori* designed frequency seriously limits their integration into many devices and systems.

Recently, a gold-helix photonic metamaterial [19,20] was introduced and investigated as a compact and broadband circular polarizer. For light propagating along the helix axis, the structure was demonstrated to block circular polarization with the same handedness as the helices but to transmit the other, for a frequency range exceeding one octave. At the same time, three-dimensional bichiral plasmonic crystals [21,22], tapered helices [23], and multi-helical structures [24,25] have also been conceived and shown to further improve the performance of circular polarizers. However, the complex structure design and

*o.hess@imperial.ac.uk

 

metallization make them challenging to be realized at arbitrary frequencies, for example, in the terahertz (THz) region. Although direct-laser two-photon absorption writing [19–23] and electroless plating [26] can provide an effective method, there are still restrictions in meeting requirements of practical applications such as the manufacturing of large areas or the need of a substrate, which may limit the useful spectral range.

Twisted metamaterials [27,28] are proposed based on stacked planar metasurfaces featuring parallel metallic rods realized with conventional lithographic techniques, suitably rotated from one layer to the next, to achieve the broadband circular-polarization selectivity. They are much closer to practical applications and allow for much larger sample footprints due to an inherently simpler fabrication process. However, although very elegant in their design, such twisted stacked metasurfaces so far still cannot quite match the performance of helix-based metamaterials, as their extinction ratio is not yet high enough in four-layer structures. Although higher extinction ratios can be achieved by means of seven or more layers of twisted structures, as shown in simulation, the fabrication becomes increasingly complex.

Lately, a miniature chiral beam splitter based on gyroid-photonic crystals was demonstrated to discriminate RCP and LCP light in a narrow band around 1.5-$\mu$m wavelength with a transmission of almost 50% [29].

As an alternative route to realizing high-contrast and broadband circular-dichroic properties, we propose a chiral metafoil that builds on the well-known metafoil concept [30–33]. It combines the upright *S*-string architecture [34] with the distinctive feature of metallic transverse interconnects to form a self-supported, locally stiff, globally flexible space grid. As spacings of both interconnecting lines and *S* strings can be varied, we distinguish between $pSX$ metafoils where $p = 1, 2, 3, \ldots$ and $X = E$ or $P$ stand for the number of *S* periods between subsequent interconnecting lines and for equidistant ($E$) or pairwise ($P$) grouped *S* strings [31,32], respectively. A variety of metafoils exhibiting $1 \leq p \leq 4$ and $X$ either $E$ or $P$ show a strong left-handed magnetic resonance peak between 3 and 4.5 THz that gives rise to a high transmission of electromagnetic waves [31,32]. The platform of the metafoil is further extended to yield functional multiband metafoils that are experimentally and numerically demonstrated to achieve simultaneously negative permittivity and negative permeability responses at multiple frequencies [35] as well as crossed metafoils that are polarization-independent left-handed metamaterials [36]. The chiral metafoil as introduced here is an all-metal, self-supported, free-standing chiral metamaterial assembled from simple half-loop structures that feature the same handedness. It can be derived from a conventional $1SE$ metafoil by simply shifting interconnecting lines by half a unit cell length from row to row. Because of the direct coupling among these connected structures, the chiral metafoil can effectively operate as a three-dimensional structure with a broadband optical response. Its global flexibility lends it a further degree of freedom for shaping optical surfaces, most readily, with cylindrical contours of circular, elliptic, parabolic, and hyperbolic shape. This feature could be useful in relation to cylindrical-source geometries as they occur, e.g., when light is scattered from a particle beam and its detection needs to be discriminated according to its circular polarization. Furthermore, it may play a role when circular polarizers need to conform to curved surfaces, the design of which is dictated from other considerations.

In this paper, we demonstrate experimentally and numerically that high-contrast broadband circular-polarization selectivity can be achieved by a chiral metafoil in the THz region. The bandwidth of the dichroic response is about one octave at a center frequency of 2.4 THz, the ratio between LCP and RCP light is about 700% with the maximum transmittance being approximately 70%. Chiral metafoils may be manufactured by imprinting and hot embossing in any frequency range, enabling cost-effective mass manufacture, and may so be extended to the higher infrared and optical frequencies as well, thus enabling their direct integration into current devices and systems.

## II. METHODS

### A. Sample fabrication

For the initial UV photomask, a soda-lime blank (Nanofilm, Wetlake Village, California) with 100-nm-thick chromium and a 530-nm-thick layer of AZ1518 photoresist is patterned by a direct-write laser system (Heidelberg Instruments uPG 101). Three optical masks, each carrying the design patterns of the individual layers and alignment marks, are used in the photolithography process. A 500-$\mu$m-thick silicon wafer is cleaned and covered with thin layers of Cr/Au (100 nm/50 nm) as an adhesion and plating base, respectively. A 17-$\mu$m-thick AZ9260 resist is deposited by spin coating and then exposed by UV light in a Mask & Bond Aligner (Karl Suss, MA8/BA6). After resist development, the remaining resist mold is used for gold electroplating to build up a 17-$\mu$m-thick gold structure. Then, another 50-nm gold layer is sputtered on the sample as a new plating base. The same process sequence is repeated to obtain the second and third layers of the three-dimensional structure. Precise alignment of photomasks with respect to the already-processed structure on the substrate is critical during this process. Next, the AZ9260 resist and Au plating bases are removed step by step using acetone and gold etchant. Finally, the whole structure is released from the silicon substrate by Cr etching to form all-metal, free-standing, chiral metamaterials.

### B. Optical characterization

The fabricated chiral metafoil is characterized by terahertz time-domain spectroscopy (THz TDS) in a

nitrogen-purged chamber with a relative humidity less than 5%. Time-domain spectra of the co- and cross-polarization states of the chiral metafoil are measured in transmission mode by employing polyethylene polarizers (TYDEX) in front of and behind the chiral metafoil. Transmission coefficients of the circularly polarized waves are then obtained from linear measurements using the following equation:

$$\begin{pmatrix} T_{++} & T_{+-} \\ T_{-+} & T_{--} \end{pmatrix} = \frac{1}{2}\begin{pmatrix} (T_{xx}+T_{yy})+i(T_{xy}-T_{yx}) & (T_{xx}-T_{yy})-i(T_{xy}+T_{yx}) \\ (T_{xx}-T_{yy})+i(T_{xy}+T_{yx}) & (T_{xx}+T_{yy})-i(T_{xy}-T_{yx}) \end{pmatrix},$$

where the first and second subscripts refer to the incident and transmitted wave, + and − refer to the right-handed and left-handed circularly polarized waves, and $x$ and $y$ refer to the two linearly polarized waves with the electric field polarized along two orthogonal directions.

## III. RESULTS

### A. Configuration of chiral metafoils

The construction principle of our chiral metafoil is illustrated in Fig. 1. A simple rod, with a length of $l = 90$ $\mu$m, width of $w = 30$ $\mu$m, and thickness of $t = 17$ $\mu$m can produce a strong, resonant anisotropy within the plane while being strictly nonchiral. The LCP and RCP transmissions are expected to be identical for normal incidence at all frequencies. Fractional-screw-like structures are made by stacking and connecting three of such planar nonchiral rods with a rotation angle of 90° between them, thus forming the basic building blocks of chiral metafoils. Based on the direction of rotation from top to bottom, we define the right-turn structure and left-turn structure, respectively. By this specific rotation between adjacent layers, 3D chirality is achieved in these fractional-screw-like structures.

Stacking a large number of rods with sequential rotation is one way to achieve the broad operation bands and high-extinction ratios [27]. In contrast, the chiral metafoil we propose uses a different route: handed structures with the same handedness are assembled in the form of a closely coupled array to realize the desired high-contrast and broadband properties. Thereby, a right-handed chiral metafoil's molecule is assembled by combining two right-turn structures as illustrated in Fig. 1(a). Many right-handed chiral metafoil's molecules are then joined together to form the right-handed chiral metafoil. The same construction principle applies to left-handed chiral metafoils as shown altogether in Fig. 1(b) where, in chemical terminology, line (b) represents the enantiomer version of the structures of line (a) [37]. Topologically, the unit cell corresponds to two split rings

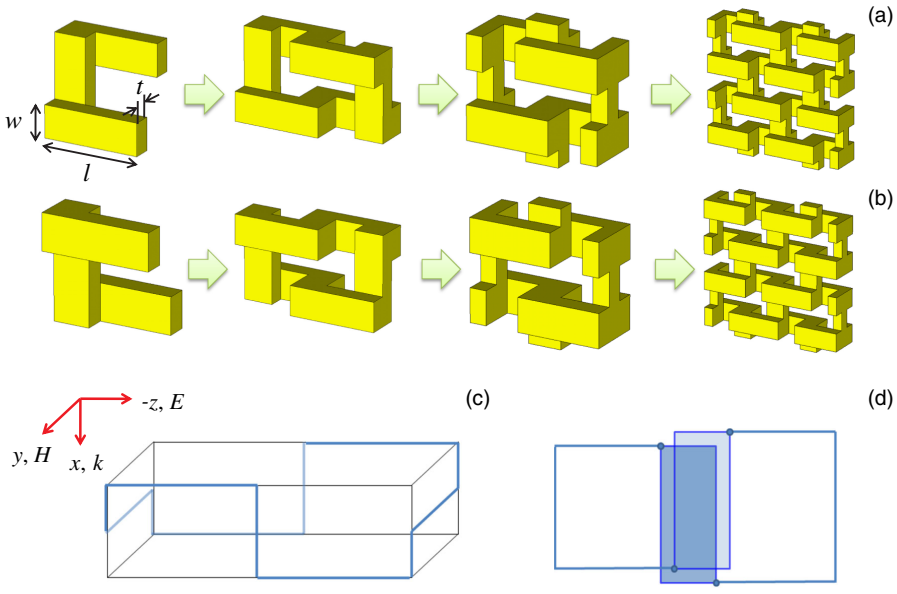


FIG. 1. The configuration of right-handed (a) and left-handed (b) chiral metafoils. Actual values of parameters $w$, $l$, $t$ are $l = 90$ $\mu$m, $w = 30$ $\mu$m, and $t = 17$ $\mu$m. A wire frame schematic (c) and a topological schematic (d) of chiral metafoil's unit cell.

cross coupled to a common capacitor as schematically illustrated in Figs. 1(c) and 1(d) depicting the corresponding wire frame and topological diagrams of the unit cell, respectively. In simplest terms, the structure of a chiral metafoil results from a shift of the interconnecting lines of a conventional 1*SE* metafoil by half a unit cell length from row to row.

### B. Numerical simulations

Simulations of chiral metafoils are performed by using the frequency domain solver of the commercial CST Microwave Studio software, which implements a finite element method to determine reflection and transmission properties. In the simulations, the unit cell boundary condition is applied and the circularly polarized eigenwaves are directly used. Gold is modeled as a lossy metal with conductivity $\sigma = 4.09 \times 10^7$ S m$^{-1}$.

Figures 2(a) and 2(c) show schematic 3D diagrams of the right-handed and left-handed chiral metafoils, and Figs. 2(b) and 2(d) show the corresponding simulated transmission spectra of the LCP and RCP waves, respectively. For right-handed chiral metafoils, the RCP waves are preferentially transmitted within the bandwidth of operation from about 1.5 to 3.4 THz, whereas the LCP waves are almost blocked. The associated (numerically simulated) circular dichroism, which reflects the difference between the transmission spectra of two circular polarizations (the maximum difference divided by the maximum transmission), can reach about 95% in the chiral metafoil. This value clearly exceeds the previously reported performance of the seven-layer rotated metasurfaces [27]. As expected from symmetry, the left-handed chiral metafoils show the same transmission spectra, except that the spectra for the LCP and RCP waves are exchanged.

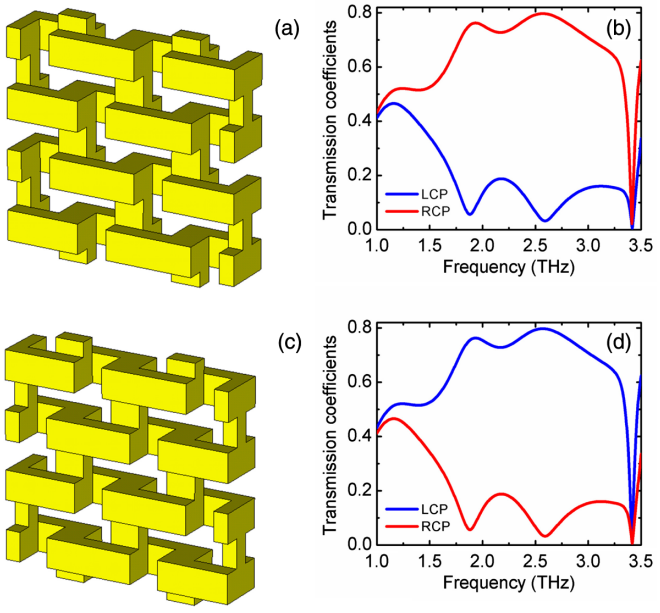


FIG. 2. Simulation results of broadband chiral metafoils. 3D schematics of right-handed (a) and left-handed (c) chiral metafoils. The simulated transmission spectra of the LCP and RCP waves for the right-handed (b) and left-handed (d) chiral metafoils at normal incidence.

### C. Experimental realization and characterization

The terahertz chiral metafoils are manufactured using three-level photolithography with precise alignment and three repeated gold-electroplating steps with accurate thickness control. All fractional-screw-like structures are linked together and self-supported, assuring a remarkably high degree of robustness of our chiral metafoils. After being released from the substrate, the chiral metafoils turn into all-metal, self-supported, free-standing metamaterials (see Sec. II). Figure 3(a) shows photographs of flat as well as deliberately bent chiral metafoils. The useful window of chiral metafoils that is available for transmission is $10 \times 10 \times 0.051$ mm$^3$ ($L \times W \times H$). Figures 3(b)–3(d) show scanning electron microscope (SEM) images of these fabricated metafoils.

The high-contrast and broadband properties of chiral metafoils are experimentally demonstrated by THz TDS [38,39] (see Sec. II). Figures 3(e)–3(h) show SEM images and the measured transmission spectra for the two circularly polarized terahertz waves in the right-handed and left-handed chiral metafoils, respectively. As predicted by simulations, our terahertz chiral metafoils experimentally support circular-polarization selectivity over a broad bandwidth from about 1.5 to 3.4 THz, and circular dichroism can experimentally reach about 85%. The measured results in Figs. 3(f) and 3(h) are in very good agreement with the simulated results in Figs. 2(b) and 2(d). Some small discrepancies between experiments and simulations are mainly due to the tolerances in the fabrication and characterization. For comparison purposes, Figs. 3(i) and 3(j) show that a conventional equidistant 1*SE* metafoil does not exhibit any circular dichroism at all. As, in this case, there are equal numbers of identical right-handed and left-handed unit cells, the circular-polarization selectivity arising from them is completely canceled out mutually, making the measured transmission spectra of RCP and LCP identical. In chemical terminology, this equal distribution of right-handed and left-handed unit cells corresponds to the racemic modification [37]. In Figs. 4(a) and 4(b), we show the influence of the capacitor in the ring and the thickness of the conductors on the transmission spectra. We observe that increasing the capacitance leads to a narrower and higher broadband peak, whereas an enlargement of the conductor thickness shifts the peak to higher frequencies. This potential of varying parameters clearly offers an additional degree of designing capability with respect to tuning the frequency and spectral shape.

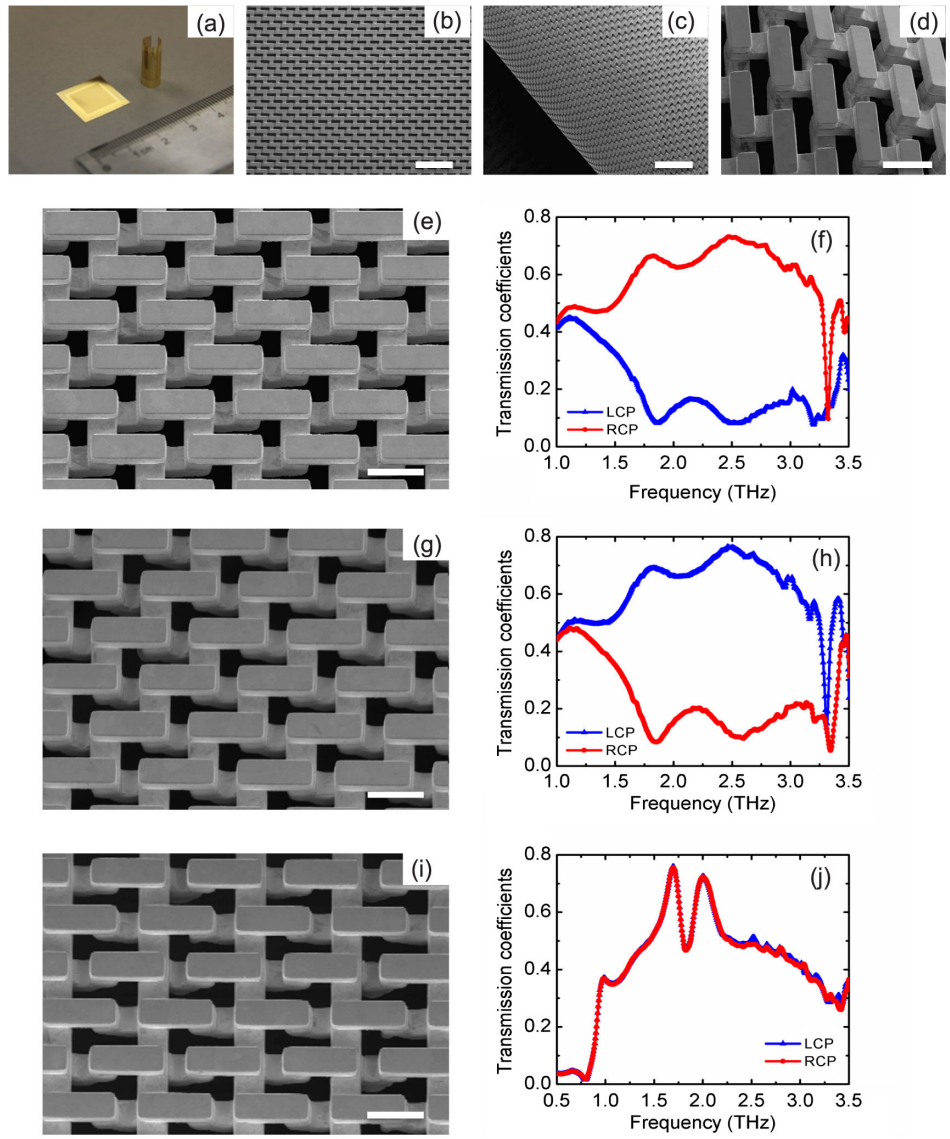


FIG. 3. Experimental demonstration of broadband chiral metafoil. (a) Photographs of the flat and deliberately bent chiral metafoils. (b)–(d) Scanning-electron-microscopy images of the fabricated chiral metafoils; the scale bar is 300 $\mu$m in (b) and (c), 80 $\mu$m in (d), respectively. (e) Scanning-electron-microscopy image of the right-handed chiral metafoil; the scale bar in (e) is 80 $\mu$m. (f) The measured transmission spectra of LCP and RCP waves for the right-handed chiral metafoil. (g) Scanning-electron-microscopy image of the left-handed chiral metafoil; the scale bar in (g) is 80 $\mu$m. This structure is an enantiomer of (e). (h) The measured transmission spectra of LCP and RCP waves for the left-handed chiral metafoil. (i) Scanning-electron-microscopy image of the conventional 1*SE* metafoil; the scale bar in (i) is 80 $\mu$m. (j) The measured transmission spectra of LCP and RCP waves for the 1*SE* metafoil showing that the conventional 1*SE* metafoil does not exhibit any dichroism at all as it is the racemic modification of structures (e) and (g).

## IV. DISCUSSION

In a conventional metafoil, the topology of a unit cell corresponds to two oppositely inclined split rings cross coupled via a common capacitor. Our chiral metafoil is structurally very similar, but for a small, yet crucial difference: the interconnecting coupling lines are shifted by half of an *S* length from row to row. This difference is crucial, as it creates the right- or left-handed structure. Indeed, looking at the structure depicted in Figs. 1(a) or 1(b), we can see that, starting at any point of the structure and following the path of a propagating wave going into the metafoil, the path describes a right-handed screw in Fig. 1(a) or a left-handed screw in Fig. 1(b). The shape of the spectral response of a chiral metafoil is completely different from the conventional metafoil. Whereas the latter exhibits a magnetic negative-$\mu$ resonance which has a relative bandwidth of about 10%, the present chiral metafoil, in contrast, features a much broader circular-polarization-selective passband with a spectral width of more than one octave superposed on which magnetic resonant peaks can be observed.

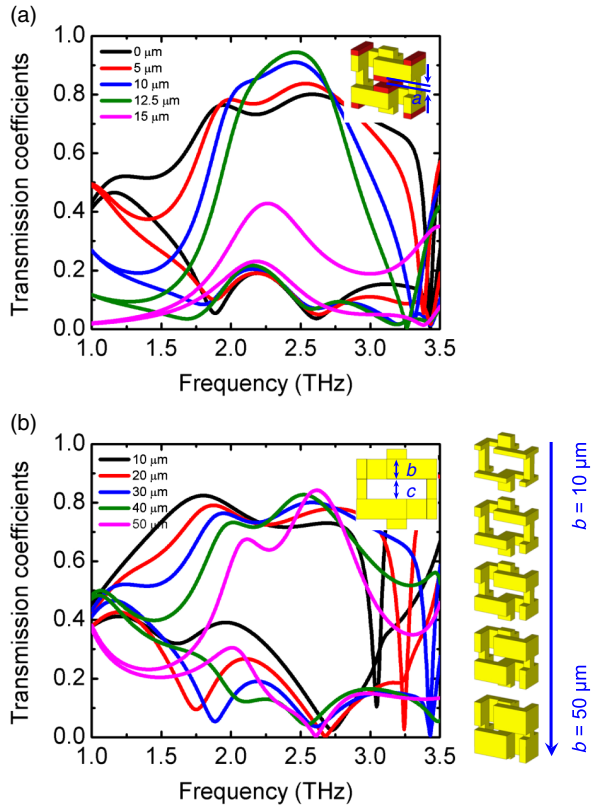


FIG. 4. The influence of capacitance and conductor thickness. (a) $a$ changes from 0 to 15 $\mu$m. (b) Unit length $u = 2b + 2c = 120$ $\mu$m keeps constant while $b$ changes from 10 to 50 $\mu$m.

To describe the basic excitation of the broadband chiral metafoil, let us consider a plane circularly polarized wave incident on the chiral metafoil in the $x$ direction. Let us further assume the incident circularly polarized wave to be decomposed, as usual, into two orthogonal, linearly polarized waves. There is thus a phase shift of $\pi/2$ or $-\pi/2$ between the orthogonal components to produce right-circular or left-circular light, respectively [40]. We further assume the electric-field vector of the leading component to be oriented in the direction of the $S$ strings of the metafoil ($z$ direction). Then, the related $H$ vector will point normal to the loops ($y$ direction) and excite them fully magnetically. This magnetic induction leads to an $LC$ oscillation. The current influenced by the electric field thus flows in the same direction. The electric-field vector of the phase-shifted orthogonal component, the trailing wave, will then point in a direction normal to the loops ($y$ direction) and the related $H$-field vector will be along the $S$ strings ($z$ direction). In this case, the loop area projected onto a plane perpendicular to $H$ is comparatively small, so magnetic induction plays a smaller role. To understand the dichroism, we note that, depending on the material, the electric field of the incident wave sees a right-handed or left-handed inclined split ring. It is the interaction with this inclined split ring that brings about the observed circular dichroism. During the first half wave of the leading component, the electric field excites a current along the top rods of the structure such that the capacitor between rods is charged. After the first quarter wave, the orthogonal trailing component helps to direct the current further along the split ring combined with the discharge of the capacitor, provided the circular polarization corresponds to the handedness of the inclined split ring. After the first half wave, the direction of electric excitation and the direction of the current flow are inverted, and, due to the axial symmetry of the unit cell, the second half of the ring current is performed such that, after one wave, one circular current flow is completed. If the handedness of the inclined split rings and the circular polarization do not match, the field of the trailing wave excites a current opposite to the discharge current of the capacitor, thus partly compensating current flows and reducing transmission. While we have argued that the magnetic field of the trailing component can barely excite loops, the magnetic field of the leading component does. However, this does not distinguish between right- or left-circular excitation and, thus, plays no role in the circular-polarization selectivity. In detail, during the first quarter wave of the leading component, the electric field and the induced electromagnetic field point to the same direction while they are opposite in the second quarter. Depending on the position of the spectral resonance, the magnetically induced current can be larger or smaller, thus leading to the waviness of the transmission spectra we observe.

While having some similarities to helical [19] as well as to twisted [27] metamaterials, our chiral metafoil is, however, distinctly different from both. The chiral-metafoil features inclined split rings that may also be called fractional screws. The crucial property is that the two fractional screws making up a unit cell are oriented such that they alternatingly accommodate the two half waves of the incident light as illustrated in Fig. 1, thus supporting the propagation of a like-handed wave. In contrast, in a helix, short circuiting currents are set up in the like-handed case that block the incoming wave [19]. The thickness of the layer filled with helices—or the height of a helix—is about one-half wavelength. Owing to the geometric difference, the response of the chiral metafoil is thus completely different from that of the gold helix as it transmits the wave of like handedness. Compared to twisted metamaterials, the chiral metafoil is similarly composed of metal rods that have orientations differing by 90° from each other. However, in the chiral metafoil these rods are galvanically coupled, not only capacitively or inductively as between insulated layers in twisted metamaterials (which are basically a stack of wire grid filters with different angular position of each layer). Considering a single layer of a twisted metamaterial, the $E$-field vector perpendicular to the rods is transmitted. As the next layer is rotated, the transmitted $E$-field vector also needs to rotate. The

handedness of the rod rotation and the $E$-field-vector rotation, then, is identical. Therefore, they pass like-handed polarization. In chiral metafoils, however, the selectivity between right- and left-handed circular polarizations is significantly larger than in twisted metamaterials. Moreover, both helical and twisted metamaterials need substrates and/or embedding matrices. This may restrict the useful spectral range. In the case of the twisted metamaterial, the optimum distance between layers is $L = 120$ nm for a useful spectral range of 600–1400 nm, leading to a total thickness of about one wavelength. It thus does not seem immediately obvious that and how this concept may be extended to larger wavelengths into the THz range.

Compared with the gyroid-photonics crystal [29], the chiral metafoil is fundamentally different in at least two aspects, namely, the bandwidth and the thickness. Regarding the former, the chiral metafoil features a bandwidth of about one octave, whereas the gyroid-photonics crystal is reported to have a relative bandwidth of about $1/60$. So, the relative bandwidth of the chiral metafoil is larger by a factor of 120. As for the thickness, the chiral metafoil is 51 $\mu$m thick and the shortest wavelength in the bandpass is 88 $\mu$m, so it is less than one wavelength thick in the propagation direction, whereas the gyroid-photonics crystal prism is about 32 wavelengths thick at the point of incidence. As a corollary, we note here that due to their small thickness, the chiral metafoils should be regarded in the spirit of an effective metasurface rather than a bulk metamaterial for which one would be able to identify an effective chiral parameter $\kappa$.

While the chiral metafoils studied in this paper were produced by means of three-level photolithography, an important aspect is that they may also be manufactured by plastic molding. Two parts of either a mold insert for injection molding or two parts of a hot embossing die yield the plastic metafoil structure. Note that such plastic structures can be metallized by sputter deposition of the desired metal. Although here implemented at terahertz frequencies, the techniques of imprinting or hot embossing suggest that the chiral-metafoil concept can be extended to higher infrared and optical frequencies, with cost-effective mass manufacture.

## V. CONCLUSION

We have designed, manufactured, and demonstrated broadband chiral metafoils that exhibit a high-contrast circular-polarization selectivity over a bandwidth of about one octave (1.7–3.4 THz). This performance is achieved by a simple design variation of the well-known metafoil, namely, replacing straight interconnecting lines by alternating ones. In chemical terminology, we may regard the "molecules" in LCP and RCP chiral metafoils as enantiomers and, consequently, the conventional metafoil as a corresponding racemic modification. All of metafoil structures can be fabricated by means of the well-established three-level photolithography and gold-electroplating technique. As the geometric structure of metafoils is amenable to hot embossing or nanoimprinting, the results achieved hold promise to enable extension of the frequency range up to the visible red with gold by reducing geometric parameters suitably. Owing to the all-metal structure of metafoils, there are no dielectrics of substrates or embedding matrices that could lead to a redshift of the frequencies. Hence, full use can be made of the accessible spectral range that extends up to about 450 THz (667 nm) before limiting plasmonic effects are expected to set in [41]. An additional benefit of hot embossing and nanoimprint processes is a ready access to cost-effective mass manufacture. In this way, broadband circular-polarization filters may be realized over a spectral range spanning almost 3 orders of magnitude from THz to the visible red, covering, in particular, the important infrared "fingerprint" range (12–120 THz) that is routinely used for infrared molecular spectroscopy including related methods such as vibrational circular dichroism.

## ACKNOWLEDGMENTS

This work is funded by the National Research Foundation, Prime Minister's Office, Singapore under its Competitive Research Program (CRP Grant No. NRF-CRP10-2012-04) and NUS Core Support C-380-003-003-001. Support by the Leverhulme Trust is gratefully acknowledged.

[1] K. Nakanishi, N. Berova, and R. W. Woody, *Circular Dichroism: Principles and Applications* (VCH, Weinheim, Germany, 1994).

[2] I. V. Lindell, A. H. Sihvola, S. A. Tretyakov, and A. J. Viitanen, *Electromagnetic Waves in Chiral and Bi-isotropic Media* (Artech House Publisher, Boston, 1994).

[3] S. Tretyakov, A. Serdyukov, I. Semchenko, and A. Sihvola, *Electromagnetics of Bi-anisotropic Materials: Theory and Applications* (Gordon and Breach Science, London, 2001).

[4] J. B. Pendry, A chiral route to negative refraction, Science **306**, 1353 (2004).

[5] E. Plum, J. Zhou, J. Dong, V. A. Fedotov, T. Koschny, C. M. Soukoulis, and N. I. Zheludev, Metamaterial with negative index due to chirality, Phys. Rev. B **79**, 035407 (2009).

[6] S. Zhang, Y.-S. Park, J. Li, X. Lu, W. Zhang, and X. Zhang, Negative refractive index in chiral metamaterials, Phys. Rev. Lett. **102**, 023901 (2009).

[7] M. Decker, M. Ruther, C. E. Kriegler, J. Zhou, C. M. Soukoulis, S. Linden, and M. Wegener, Strong optical activity from twisted-cross photonic metamaterials, Opt. Lett. **34**, 2501 (2009).

[8] M. Decker, R. Zhao, C. M. Soukoulis, S. Linden, and M. Wegener, Twisted split-ring-resonator photonic metamaterial with huge optical activity, Opt. Lett. **35**, 1593 (2010).

[9] J. Zhou, J. Dong, B. Wang, T. Koschny, M. Kafesaki, and C. M. Soukoulis, Negative refractive index due to chirality, Phys. Rev. B **79**, 121104 (2009).

[10] Z. Li, K. B. Alici, E. Colak, and E. Ozbay, Complementary chiral metamaterials with giant optical activity and negative refractive index, Appl. Phys. Lett. **98**, 161907 (2011).
[11] R. Zhao, L. Zhang, J. Zhou, T. Koschny, and C. M. Soukoulis, Conjugated gammadion chiral metamaterial with uniaxial optical activity and negative refractive index, Phys. Rev. B **83**, 035105 (2011).
[12] J. Wu, B. Ng, S. P. Turaga, M. B. H. Breese, S. A. Maier, M. Hong, A. A. Bettiol, and H. O. Moser, Free-standing terahertz chiral meta-foils exhibiting strong optical activity and negative refractive index, Appl. Phys. Lett. **103**, 141106 (2013).
[13] R. Zhao, T. Koschny, and C. M. Soukoulis, Chiral metamaterials: Retrieval of the effective parameters with and without substrate, Opt. Express **18**, 14553 (2010).
[14] G. Kenanakis, R. Zhao, A. Stavrinidis, G. Konstantinidis, N. Katsarakis, M. Kafesaki, C. M. Soukoulis, and E. N. Economou, Flexible chiral metamaterials in the terahertz regime: A comparative study of various designs, Opt. Mater. Express **2**, 1702 (2012).
[15] S. Zhang, J. Zhou, Y.-S. Park, J. Rho, R. Singh, S. Nam, A. K. Azad, H.-T. Chen, X. Yin, A. J. Taylor, and X. Zhang, Photoinduced handedness switching in terahertz chiral metamolecules, Nat. Commun. **3**, 942 (2012).
[16] C. M. Soukoulis and M. Wegener, Past achievements and future challenges in the development of three-dimensional photonic metamaterials, Nat. Photonics **5**, 523 (2011).
[17] Y. Liu and X. Zhang, Metamaterials: A new frontier of science and technology, Chem. Soc. Rev. **40**, 2494 (2011).
[18] Q. Hong, T. X. Wu, X. Zhu, R. Lu, and S.-T. Wu, Designs of wide-view and broadband circular polarizers, Opt. Express **13**, 8318 (2005).
[19] J. K. Gansel, M. Thiel, M. S. Rill, M. Decker, K. Bade, V. Saile, G. V. Freymann, S. Linden, and M. Wegener, Gold helix photonic metamaterial as broadband circular polarizer, Science **325**, 1513 (2009).
[20] J. K. Gansel, M. Wegener, S. Burger, and S. Linden, Gold helix photonic metamaterials: A numerical parameter study, Opt. Express **18**, 1059 (2010).
[21] M. Thiel, M. S. Rill, G. V. Freymann, and M. Wegener, Three-dimensional bi-chiral photonic crystals, Adv. Mater. **21**, 4680 (2009).
[22] A. Radke, T. Gissibl, T. Klotzbücher, P. V. Braun, and H. Giessen, Three-dimensional bichiral plasmonic crystals fabricated by direct laser writing and electroless silver plating, Adv. Mater. **23**, 3018 (2011).
[23] J. K. Gansel, M. Latzel, A. Frölich, J. Kaschke, M. Thiel, and M. Wegener, Tapered gold-helix metamaterials as improved circular polarizers, Appl. Phys. Lett. **100**, 101109 (2012).
[24] Z. Yang, M. Zhao, and P. Lu, How to improve the signal-to-noise ratio for circular polarizers consisting of helical metamaterials, Opt. Express **19**, 4255 (2011).
[25] J. Kaschke, J. K. Gansel, and M. Wegener, On metamaterial circular polarizers based on metal *N*-helices, Opt. Express **20**, 26012 (2012).
[26] Y. Yan, M. I. Rashad, E. J. Teo, H. Tanoto, J. Teng, and A. A. Bettiol, Selective electroless silver plating of three-dimensional SU-8 microstructures on silicon for metamaterials applications, Opt. Mater. Express **1**, 1548 (2011).
[27] Y. Zhao, M. A. Belkin, and A. Alù, Twisted optical metamaterials for planarized ultrathin broadband circular polarizers, Nat. Commun. **3**, 870 (2012).
[28] Y. Zhao, J. Shi, L. Sun, X. Li, and A. Alù, Alignment-free three-dimensional optical metamaterials, Adv. Mater. **26**, 1439 (2014).
[29] M. D. Turner, M. Saba, Q. Zhang, B. P. Cumming, G. E. Schröder-Turk, and M. Gu, Miniature chiral beamsplitter based on gyroid photonic crystals, Nat. Photonics **7**, 801 (2013).
[30] H. O. Moser, L. K. Jian, H. S. Chen, M. Bahou, S. M. P. Kalaiselvi, S. Virasawmy, S. M. Maniam, X. X. Cheng, S. P. Heussler, S. B. Mahmood, and B.-I. Wu, All-metal self-supported THz metamaterial—The meta-foil, Opt. Express **17**, 23914 (2009).
[31] H. O. Moser, L. K. Jian, H. S. Chen, M. Bahou, S. M. P. Kalaiselvi, S. Virasawmy, X. X. Cheng, A. Banas, K. Banas, S. P. Heussler, B.-I. Wu, W. B. Zhang, S. M. Maniam, and W. Hua, THz meta-foil—A platform for practical applications of metamaterials, J. Mod. Opt. **57**, 1936 (2010).
[32] H. O. Moser, L. K. Jian, H. S. Chen, S. M. P. Kalaiselvi, S. Virasawmy, X. X. Cheng, A. Banas, K. Banas, S. P. Heussler, M. Bahou, B.-I. Wu, W. Hua, and Z. Yi, Geometry-function relationships in meta-foils, Proc. SPIE Int. Soc. Opt. Eng. **7711**, 771119 (2010).
[33] H. O. Moser and C. Rockstuhl, 3D THz metamaterials from micro/nanomanufacturing, Laser Photonics Rev. **6**, 219 (2012).
[34] X. X. Cheng, H. S. Chen, L. Ran, B.-I. Wu, T. M. Grzegorczyk, and J. A. Kong, A bianisotropic left-handed metamaterials compose of *S*-ring resonator, PIERS Online **3**, 593 (2007).
[35] J. Wu, H. O. Moser, S. Xu, L. K. Jian, A. Banas, K. Banas, H. S. Chen, A. A. Bettiol, and M. B. H. Breese, Functional multi-band THz meta-foils, Sci. Rep. **3**, 3531 (2013).
[36] J. Wu, H. O. Moser, S. Xu, A. Banas, K. Banas, H. S. Chen, and M. B. H. Breese, From polarization-dependent to polarization-independent terahertz meta-foils, Appl. Phys. Lett. **103**, 191114 (2013).
[37] H. Beyer and W. Walter, *Lehrbuch der Organischen Chemie* (S. Hirzel Verlag, Stuttgart, 1991).
[38] D. H. Auston and K. P. Cheung, Coherent time-domain far-infrared spectroscopy, J. Opt. Soc. Am. B **2**, 606 (1985).
[39] C. A. Schmuttenmaer, Exploring dynamic in the far-infrared with terahertz spectroscopy, Chem. Rev. **104**, 1759 (2004).
[40] M. Born and E. Wolf, *Principles of Optics* (Cambridge University Press, Cambridge, U.K., 2005).
[41] S. Tretyakov, On geometrical scaling of split-ring and double-bar resonators at optical frequencies, Metamaterials **1**, 40 (2007).